Beam energy dependence of pseudorapidity distributions of charged particles produced in relativistic heavy-ion collisions

Sumit Basu and Tapan K. Nayak
Variable Energy Cyclotron Centre, Kolkata 700064, India

Kaustuv Datta
Department of Physics, Reed College, Portland, Oregon 97202, USA
(Received 18 January 2016; revised manuscript received 19 March 2016; published 6 June 2016)

Heavy-ion collisions at the Relativistic Heavy Ion Collider at Brookhaven National Laboratory and the Large Hadron Collider at CERN probe matter at extreme conditions of temperature and energy density. Most of the global properties of the collisions can be extracted from the measurements of charged-particle multiplicity and pseudorapidity (η) distributions. We have shown that the available experimental data on beam energy and centrality dependence of η distributions in heavy-ion (Au + Au or Pb + Pb) collisions from $\sqrt{s_{NN}} = 7.7$ GeV to 2.76 TeV are reasonably well described by the AMPT model, which is used for further exploration. The nature of the η distributions has been described by a double Gaussian function using a set of fit parameters, which exhibit a regular pattern as a function of beam energy. By extrapolating the parameters to a higher energy of $\sqrt{s_{NN}} = 5.02$ TeV, we have obtained the charged-particle multiplicity densities, η distributions, and energy densities for various centralities. Incidentally, these results match well with some of the recently published data by the ALICE Collaboration.

DOI: 10.1103/PhysRevC.93.064902

I. INTRODUCTION

The primary goal of colliding heavy ions at ultrarelativistic energies is to study nuclear matter under extreme conditions, in which hadronic matter is expected to undergo a phase transition to a new state of matter, quark-gluon plasma (QGP) [1,2]. Quantum chromodynamics (QCD), the theory of strong interactions, suggests that, at high temperatures and energy densities, nuclear matter melts down to this new phase of deconfined quarks and gluons. Recent lattice QCD calculations [3,4] indicate that the transition from hadronic matter to QGP occurs at a critical temperature of $T_C \sim 155$ MeV and a critical energy density of $\epsilon_C \sim 0.7$–1.9 GeV/fm^3. The QGP research programs at the Relativistic Heavy Ion Collider (RHIC) at Brookhaven National Laboratory and the Large Hadron Collider (LHC) at CERN are on a quest to unearth the physics of deconfinement and vacuum and to understand how matter behaved within a few microseconds after the birth of our universe. With the first phase of the beam energy scan program at the RHIC during 2010 and 2011, data for Au + Au collisions at a nucleon-nucleon (NN) center-of-mass energy ($\sqrt{s_{NN}}$) from 7.7 to 200 GeV are available. The main aim of this program is to probe the onset of deconfinement and to locate the QCD critical point [5]. The LHC has collided Pb + Pb beams at $\sqrt{s_{NN}} = 2.76$ TeV during the first phase of its operation (2010 and 2011). During the first year of the second phase of the LHC operation in 2015, data for Pb + Pb collisions at $\sqrt{s_{NN}} = 5.02$ TeV were collected. Thus with the combination of the RHIC and the LHC, high-quality data for heavy-ion collisions have now been available over quite a broad energy range. At the same time a large number of models have emerged which attempt to analyze and explain the data and extract physical parameters [6–10].

Global observables such as charged-particle multiplicity distributions, pseudorapidity (η) distributions, momentum spectra, particle ratios, size of the fireball, and azimuthal anisotropy provide the majority of the valuable information for thermal and chemical analysis of the freeze-out conditions [11,12]. The η distribution of charged particles is one of the most basic and most important observables to characterize the colliding system and to understand the phase transition. All the observables in heavy-ion collisions scale with the number of particles. So the knowledge of the particle density is essential for validating any measurement. The pseudorapidity particle density at midrapidity, along with the transverse energy per particle provides the energy density of the fireball using the Bjorken estimation [13]. The pseudorapidity distributions are intimately connected to the energy density of the emitting source and provide an important test bed for validating theoretical models, which attempt to describe the conditions in the early phases of the collision.

Experimental data for η distributions have been reported for all the collider energies available at the RHIC [14,15] and the LHC [16–20]. In this article, we make a compilation of some of the available data in terms of the variation of pseudorapidity distributions of charged particles with beam energy and collision centrality. We make a similar study using a multiphase transport (AMPT) model and make a comparison with the available data. In this model, different values of parton cross sections are used to explain the data at the LHC. The pseudorapidity distributions, from both data and the AMPT model, of charged particles from $\sqrt{s_{NN}} = 7.7$ GeV to 2.76 TeV are fitted by a double Gaussian function. These parameters show interesting trends as a function of beam energy. Extrapolating the parameters to higher energies, we obtain the η distribution for $\sqrt{s_{NN}} = 5.02$ TeV. It is observed that the pseudorapidity density at midrapidity matches well with the recently reported data from the ALICE Collaboration [21]. Furthermore, we extract the value of the initial energy density for collisions at $\sqrt{s_{NN}} = 5.02$ TeV.

The paper is organized as follows. In Sec. II, we discuss the AMPT model which is used to compare the data results. In Sec. III, we present the compilation of pseudorapidity distributions for data and for the AMPT model. In Sec. IV, we make an analysis of the shapes of the pseudorapidity distributions and present the results of the fit parameters. The energy dependence of charged-particle multiplicity densities, pseudorapidity distributions, and energy densities are presented. We conclude the paper with a summary in Sec. VI.

II. AMPT SETTINGS

The AMPT model [22] provides a framework to study relativistic heavy-ion collisions. It incorporates essential stages of heavy-ion collisions from the initial condition to the final observables on an event-by-event basis, including the parton cascade, hadronization, and the hadron cascade [23–25]. The model can generate events in two different modes: (a) default and (b) string melting (SM). Initial conditions for both the modes are taken from HIJING [26], where two Woods-Saxon type radial density profiles are taken for colliding nuclei. The multiple scattering among the nucleons of two heavy-ion nuclei is governed by the eikonal formalism. The particle production has two distinct sources, from hard and soft processes, depending on the momentum transfer among partons. In the default mode, energetic partons cascade through Zhang's parton cascade (ZPC) before the strings and partons are recombined and the strings are fragmented via the Lund string fragmentation function,

$$f(z) \propto z^{-1}(1-z)^{a} \exp\left(-bm_T^2/z\right), \tag{1}$$

where a and b are the Lund string fragmentation function parameters, taken to be 0.2 and 2.2. The ART model (a relativistic transport model for hadrons) [27] is used to describe how the produced hadrons will interact. In the SM mode, the strings produced from HIJING are decomposed into partons which are fed into the parton cascade along with the minijet partons. The partonic matter is then turned into hadrons through the coalescence model [28,29] and the hadronic interactions are subsequently modeled using ART. The default mode describes the evolution of collision in terms of strings and minijets followed by string fragmentation, and the SM mode includes a fully partonic QGP phase that hadronizes through quark coalescence.

In both the modes of AMPT, Boltzmann equations are solved using ZPC with a total parton elastic scattering cross section,

$$\sigma_{gg} = \frac{9\pi\alpha_s^2}{2\mu^2}\frac{1}{1+\mu^2/s} \approx \frac{9\pi\alpha_s^2}{2\mu^2}, \tag{2}$$

where α_s is the strong coupling constant, s and t are the Mandelstam variables, and μ is the Debye screening mass. Here, α_s and μ are the key deciding factors for the multiplicity yield at a particular centrality of a given energy, and they are taken as 0.47 and 3.22, corresponding to $\sigma_{gg} = 10$ mb. It is observed that the AMPT model explains the experimental data for global observables, such as, pseudorapidity density [16], transverse momentum distribution [30], particle ratio [22], and higher harmonic anisotropic flow [30] like $v2$, and $v3$ for a wide range of collision energy. We have carried out a comparison study for different observables by varying a, b, α_s, and μ corresponding to 1.5-, 3-, 6-, and 10-mb cross sections. The model therefore provides a convenient way to investigate expectations for a variety of observables with and without a QGP phase.

III. PSEUDORAPIDITY DISTRIBUTIONS: DATA AND AMPT

Pseudorapidity distributions of charged particles have been reported by fixed target as well as collider experiments. In this article, we concentrate on the results of collider experiments at the RHIC and the LHC. In Fig. 1, we present the experimental results from the PHOBOS experiment [14] at the RHIC for central Au + Au collisions at $\sqrt{s_{NN}} = 19.6$, 62.4, and 200 GeV, and from the ALICE experiment [16] at the LHC for Pb + Pb collisions at $\sqrt{s_{NN}} = 2.76$ TeV. It is observed that the distributions are symmetric around the midrapidity as they should be, but the dip structure at $\eta = 0$ gets more prominent with the increase of collision energy. For the LHC energy, the dip increases in going from peripheral to central collisions. The magnitude of the dip depends on the particle composition of the charged particles because the dip is more prominent for heavier particles like protons and antiprotons compared to pions.

In the present study, we have generated AMPT events with the SM mode for different collision energies and collision centralities. The total parton elastic scattering cross section from 7.7 to 200 GeV (RHIC energies) is taken as $\sigma_{gg} = 10$ mb, and for 2.76 TeV (LHC energy) it is chosen to be 1.5 mb. It is observed that with these settings the AMPT model can describe the data for transverse momentum spectra and flow [30]. The results of AMPT model calculations for η distributions are superimposed on Fig. 1. The AMPT results describe the data at RHIC energies well. For $\sqrt{s_{NN}} = 2.76$ TeV, the data at midrapidity are well described by the AMPT model, but

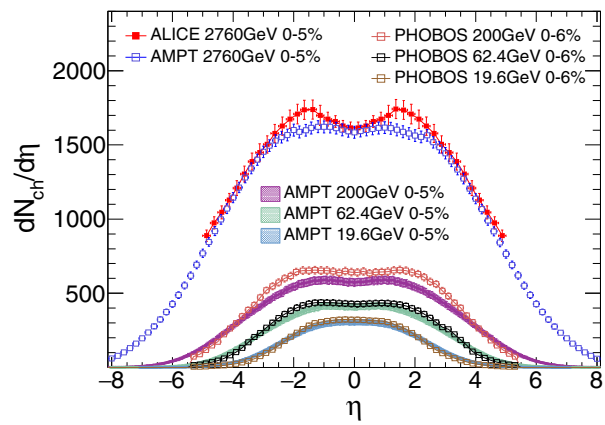

FIG. 1. Beam energy dependence of charged-particle pseudorapidity distributions. Results from the PHOBOS Collaboration [14] and the ALICE Collaboration [16,17] for central collisions are shown along with calculations from the SM mode of the AMPT model.

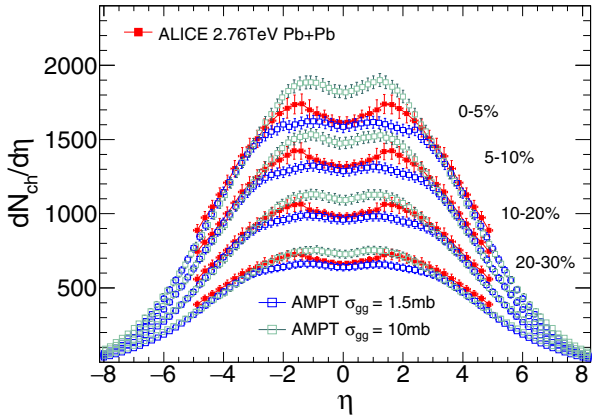

FIG. 2. Centrality dependence of charged-particle pseudorapidity distributions for Pb + Pb collisions at $\sqrt{s_{NN}} = 2.76$ TeV with the data from the ALICE experiment [16,17] and those from the AMPT model for two settings of the total parton scattering cross section (σ_{gg}).

discrepancies are observed at other η ranges especially at the peaks.

In Fig. 2, η distributions for the LHC data at $\sqrt{s_{NN}} = 2.76$ TeV for four centralities along with the AMPT model data for two different parton scattering cross sections (1.5 and 10 mb) are shown. It is seen that the AMPT results with 1.5 mb matches the midrapidity value quite well. The distributions with 10 mb match the shape of the data distribution very well, but miss the value at midrapidity. Henceforth, parton cross sections are kept at 1.5 mb for all calculations at the LHC energies.

IV. SHAPES OF PSEUDORAPIDITY DISTRIBUTIONS

Further studies have been performed to investigate the centralitywise variation of shape of the η distributions for heavy-ion collisions, ranging from 7.7 GeV to 2.76 TeV. For central Au + Au collisions at the RHIC energies, the distributions have been fitted by [31]

$$\frac{dN_{\rm ch}}{d\eta} = \frac{c\sqrt{1-1/(\alpha\cosh\eta)^2}}{1+e^{(|\eta|-\beta)/a}}, \tag{3}$$

where a, c, α, and β are fit parameters.

Figures 1 and 2 show that the η distributions exhibit a double Gaussian nature, both for experimental data and AMPT model data. This double Gaussian nature is more prominent for higher collision energies and central collisions. The shapes can be represented by double Gaussian distributions of the form,

$$A_1 e^{-(\eta_1^2/2\sigma_1^2)} - A_2 e^{-(\eta_2^2/2\sigma_2^2)}, \tag{4}$$

where the fit parameters are as follows: A_1 and A_2 are the amplitudes, η_1 and η_2 are the peak positions, and σ_1 and σ_2 are the widths of the two Gaussian distributions. The fit parameters represent the shapes of the distribution.

Both the experimental data and the AMPT distributions are fitted with the double Gaussian functional form as above and the fit parameters are extracted. The fit parameters are presented in Fig. 3 as a function of collision energy for experimental data and AMPT calculations. All the errors shown in this figure correspond to the error in fitting. The Gaussian fit parameters follow the following trends:

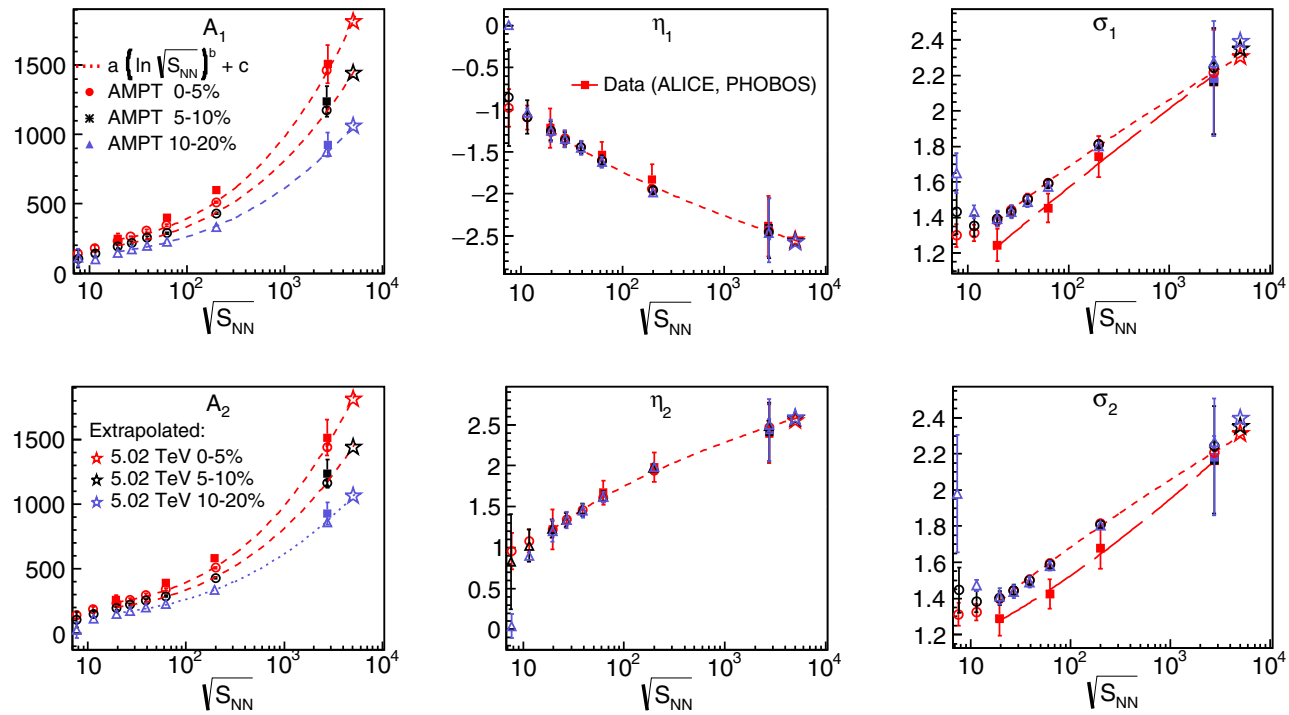

FIG. 3. Fit parameters of the double Gaussian fit to the η distributions obtained from the AMPT model for Au + Au collisions from $\sqrt{s_{NN}} = 7.7$ to 200 GeV and Pb + Pb collision at $\sqrt{s_{NN}} = 2.76$ TeV. Extrapolated values of the parameters for $\sqrt{s_{NN}} = 5.02$ TeV are also plotted in the figures.

TABLE I. Parameters of double Gaussian fits to the η distributions of Au + Au collisions from $\sqrt{s_{NN}} = 7.7$ GeV to 200 GeV and of Pb + Pb collisions at 2.76 TeV. Extrapolated parameters for $\sqrt{s_{NN}} = 5.02$ TeV are presented.

$\sqrt{s_{NN}}$ (GeV)	Centrality (%)	A_1	η_1	σ_1	A_2	η_2	σ_2
7.7	0–5	134.93 ± 25.67	−0.987 ± 0.223	1.294 ± 0.063	139.120 ± 25.05	0.225 ± 0.225	1.312 ± 0.064
	5–10	102.46 ± 63.61	−0.862 ± 0.576	1.432 ± 0.124	106.84 ± 62.43	0.825 ± 0.581	1.446 ± 0.126
	10–20	112.36 ± 61.54	−0.004 ± 0.047	1.648 ± 0.112	26.63 ± 61.93	0.042 ± 0.15	1.980 ± 0.325
11.5	0–5	178.72 ± 17.98	−1.097 ± 0.142	1.314 ± 0.045	180.78 ± 17.72	0.143 ± 0.143	1.323 ± 0.059
	5–10	142.25 ± 22.25	−1.091 ± 0.199	1.354 ± 0.059	150.42 ± 21.37	1.016 ± 0.199	1.380 ± 0.059
	10–20	100.56 ± 2.19	−1.037 ± 0.051	1.433 ± 0.035	114.22 ± 2.89	0.892 ± 0.037	1.473 ± 0.030
19.6	0–5	226.70 ± 13.19	−1.269 ± 0.098	1.383 ± 0.034	232.85 ± 12.90	1.223 ± 0.098	1.399 ± 0.034
	5–10	190.92 ± 12.63	−1.255 ± 0.111	1.392 ± 0.038	194.42 ± 12.44	1.224 ± 0.111	1.402 ± 0.038
	10–20	147.38 ± 11.90	−1.254 ± 0.132	1.393 ± 0.045	151.82 ± 11.58	1.203 ± 0.132	1.411 ± 0.045
27	0–5	260.45 ± 11.09	−1.344 ± 0.082	1.441 ± 0.029	260.59 ± 11.11	1.345 ± 0.082	1.441 ± 0.029
	5–10	218.19 ± 10.28	−1.361 ± 0.089	1.433 ± 0.032	221.92 ± 10.10	1.326 ± 0.089	1.446 ± 0.032
	10–20	171.77 ± 9.06	−1.346 ± 0.101	1.432 ± 0.036	172.96 ± 8.99	1.333 ± 0.100	1.437 ± 0.036
39	0–5	299.95 ± 9.79	−1.444 ± 0.069	1.508 ± 0.026	297.48 ± 9.87	1.457 ± 0.070	1.502 ± 0.026
	5–10	254.58 ± 8.83	−1.450 ± 0.074	1.501 ± 0.027	253.57 ± 8.87	1.455 ± 0.074	1.499 ± 0.027
	10–20	199.13 ± 7.64	−1.455 ± 0.082	1.490 ± 0.030	199.39 ± 7.62	1.450 ± 0.082	1.490 ± 0.031
62.4	0–5	341.36 ± 8.04	−1.605 ± 0.057	1.595 ± 0.022	340.53 ± 8.07	1.670 ± 0.057	1.594 ± 0.022
	5–10	288.93 ± 7.14	−1.608 ± 0.061	1.589 ± 0.023	287.59 ± 7.16	1.619 ± 0.061	1.587 ± 0.023
	10–20	225.61 ± 6.07	−1.625 ± 0.066	1.576 ± 0.026	225.71 ± 6.035	1.615 ± 0.067	1.580 ± 0.026
200	0–5	507.18 ± 6.81	−1.947 ± 0.041	1.812 ± 0.016	506.93 ± 6.77	1.940 ± 0.041	1.816 ± 0.016
	5–10	430.61 ± 5.97	−1.958 ± 0.043	1.813 ± 0.017	429.01 ± 5.99	1.965 ± 0.043	1.809 ± 0.017
	10–20	334.48 ± 4.97	−1.982 ± 0.047	1.804 ± 0.019	334.30 ± 4.97	1.979 ± 0.047	1.803 ± 0.019
2760	0–5	1458.69 ± 19.63	−2.442 ± 0.054	2.215 ± 0.022	1439.93 ± 19.75	2.471 ± 0.054	2.207 ± 0.022
	5–10	1174.33 ± 18.66	−2.462 ± 0.063	2.245 ± 0.026	1159.96 ± 18.68	2.475 ± 0.064	2.244 ± 0.026
	10–20	872.77 ± 16.66	−2.465 ± 0.075	2.274 ± 0.031	859.07 ± 16.63	2.493 ± 0.076	2.266 ± 0.032
5020	0–5	1814.52 ± 27.92	−2.554 ± 0.082	2.304 ± 0.039	1815.19 ± 28.00	2.549 ± 0.085	2.311 ± 0.040
(extrapolated)	5–10	1441.13 ± 21.23	−2.573 ± 0.091	2.348 ± 0.046	1442.23 ± 22.80	2.579 ± 0.092	2.352 ± 0.050
	10–20	1059.63 ± 17.81	−2.575 ± 0.107	2.389 ± 0.051	1061.73 ± 18.10	2.585 ± 0.110	2.395 ± 0.550

(i) The normalization parameters A_1 and A_2 increase with the increase of beam energy as per expectation. These parameters for available experimental data and the AMPT model are observed to be close together.

(ii) The values of η_1 and η_2 represent the peak positions in the η distribution. As expected, η_1 and η_2 show opposite trends with the increase of the beam energy. This means that the peak positions in η spread out more with the increase of beam energy. Note that the values of η_1 and η_2 for data and the AMPT model are close together.

(iii) The widths (σ_1 and σ_2) of the η distributions increase as a function of beam energy. For lower collision energies, the widths extracted from data are smaller than those of the AMPT model, but are close together at higher energies.

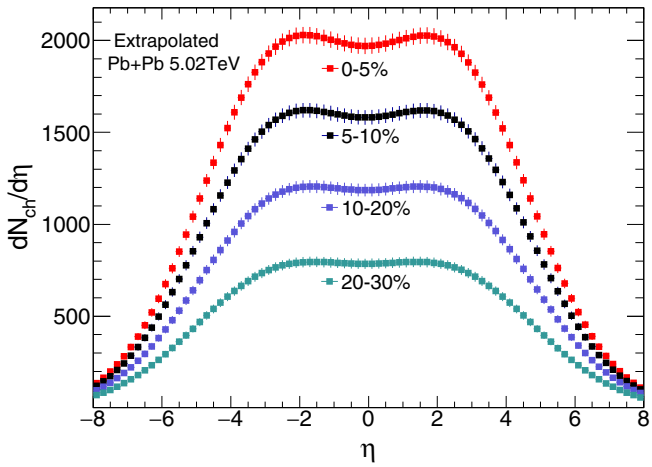

FIG. 4. η distributions for Pb + Pb collisions at $\sqrt{s_{NN}} = 5.02$ TeV for different centralities. The distributions are obtained from the extrapolated AMPT parameters from lower energies.

From the comparison of the fit parameters for data and the AMPTmodel, we observe that the AMPT model can be used as a proxy for experimental data. The AMPT points are fitted with power-law fits, shown in Fig. 3 as dashed lines. These fit values provide a way to compute the η distribution at any collision energy and centrality. Accordingly, these fit values are extended up to higher energy, viz., $\sqrt{s_{NN}} = 5.02$ TeV. The Gaussian fit parameters, along with the extrapolated values for $\sqrt{s_{NN}} = 5.02$ TeV from the AMPT model, are presented in Table I. With the extrapolated parameter set for Pb + Pb collisions at $\sqrt{s_{NN}} = 5.02$ TeV, the η distributions at different collision energies are obtained. The results are shown in Fig. 4.

V. ENERGY DEPENDENCE OF GLOBAL PARAMETERS

Parameterization of η distributions of charged particles from the AMPT model can be used to obtain energy

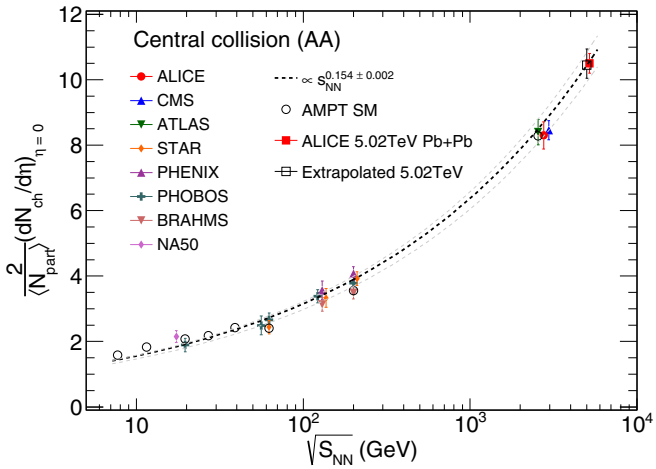

FIG. 5. Pseudorapidity density of charged particles, normalized to the number of participant pairs $[\frac{2}{\langle N_{\rm part}\rangle}(dN_{\rm ch}/d\eta)]$, plotted as a function of collision energy for central Au + Au or Pb + Pb collisions from experimental data and AMPT model data. Some of the data points are shifted along the x axis for clarity of presentation.

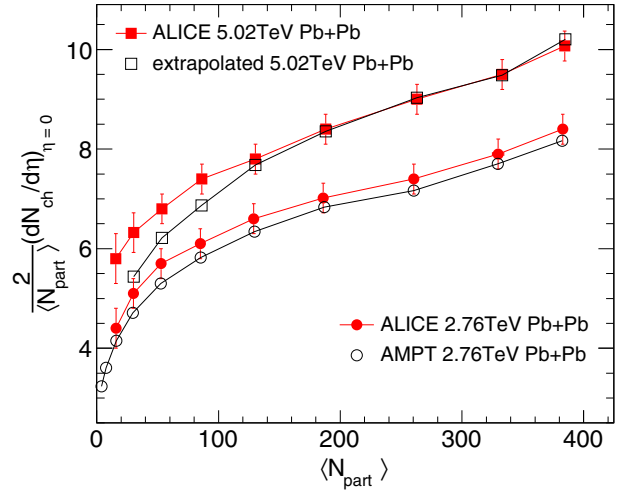

FIG. 6. Centrality dependence of $\frac{2}{\langle N_{\rm part}\rangle}(dN_{\rm ch}/d\eta)$ for Pb + Pb collisions at $\sqrt{s_{NN}} = 2.76$ and 5.02 TeV. AMPT model calculations for $\sqrt{s_{NN}} = 2.76$ TeV and extrapolations for $\sqrt{s_{NN}} = 5.02$ TeV reasonably explain the ALICE data [16,21].

dependence of several other global observables. Here we discuss the collision energy dependence of charged-particle multiplicity density at midrapidity, the centrality dependence of charged-particle multiplicity density, and the collision energy dependence of Bjorken energy density.

The quantity $2(dN_{\rm ch}/d\eta)/\langle N_{\rm part}\rangle$ gives the charged-particle multiplicity density at $\eta = 0$ scaled by the average number of participant pairs ($\langle N_{\rm part}\rangle/2$). Figure 5 shows the variation of this quantity as a function of $\sqrt{s_{NN}}$ for central (top 5% cross section) collisions. The plot shows an increase in the multiplicity density with the increase of the collision energy. The data points are taken from the PHOBOS, BRAHMS, STAR, and PHENIX experiments at the RHIC and from the ALICE, CMS, and ATLAS experiments at the LHC. The results from the AMPT model are shown by solid red points. For Pb + Pb data at 5.02 TeV, the extrapolated results from Fig. 4 have been plotted. The AMPT results explain the data quite well. A power-law fit to the AMPT model data gives the fit value as $(0.77 \pm 0.04)s_{NN}^{0.154\pm0.002}$. This matches the fit given in Ref. [21]. As shown in the figure, the extrapolated value at $\sqrt{s_{NN}} = 5.02$ TeV is close to the recently published data from the ALICE experiment [21]. The beam energy dependence of the charged-particle multiplicity density has been studied for other centralities. Power-law fits to each of the curves give the s_{NN} dependence as $s_{NN}^{0.154}$ to $s_{NN}^{0.109}$ from top central (0–5%) to peripheral (70–80%) collisions. This is consistent with the conclusion that the particle multiplicity increases faster for central collisions compared to peripheral collisions.

The centrality dependencies of the charged-particle multiplicity density have been reported for Pb + Pb collisions at $\sqrt{s_{NN}} = 2.76$ TeV [16] and 5.02 TeV [21]. As discussed earlier, the AMPT model calculations describe the data well at $\sqrt{s_{NN}} = 2.76$ TeV. By extrapolating the fit parameters from the AMPT model to higher energies of $\sqrt{s_{NN}} = 5.02$ TeV, we obtain the centrality dependence of the charged-particle multiplicity density at this energy. For central (0–5%) collisions, the multiplicity density comes out to be 1964 ± 30. The results from the experimental data and the AMPT calculations for both $\sqrt{s_{NN}} = 2.76$ and 5.02 TeV as a function of centrality are shown in Fig. 6. For Pb + Pb collisions at $\sqrt{s_{NN}} =$ 2.76 TeV, the AMPT results are within the experimental errors. For Pb + Pb collisions at $\sqrt{s_{NN}} = 5.02$ TeV, the AMPT results agree with the experimental data points, except for peripheral collisions with $\langle N_{\rm part}\rangle$ less than 130.

The charged-particle multiplicity density is normally used to estimate the initial energy density of the fireball by using the Bjorken estimation given as [13]

$$\epsilon_{\rm Bj} = \frac{1}{\pi R^2 \tau}\frac{dE_{\rm T}}{dy}, \tag{5}$$

where τ is the formation time, πR^2 is the effective area of the fireball or the overlap area of the colliding nuclei, and $dE_{\rm T}$ is the total initial energy within the rapidity window dy. The last term can be approximated as [15]

$$\frac{dE_{\rm T}}{dy} \approx \frac{3}{2}\left(\langle m_{\rm T}\rangle\frac{dN}{dy}\right)_{\pi^\pm} + 2\left(\langle m_{\rm T}\rangle\frac{dN}{dy}\right)_{K^\pm,p,\bar{p}}, \tag{6}$$

where $\langle m_{\rm T}\rangle$ is the mean transverse mass of identified particles ($\pi^\pm$, $K^\pm$, p, or $\bar{p}$). The value of τ is typically taken as 1 fm. But in the absence of experimental knowledge of τ, the energy density is expressed in terms of $\epsilon_{\rm Bj}\tau$.

The energy density, $\epsilon_{\rm Bj}\tau$, as a function of collision energy is presented in Fig. 7 for experimental results at three centralities from the NA49 [32], STAR [15,33], PHENIX [31,34,35], ALICE [36,37], and CMS [38] Collaborations. AMPT model results are superimposed for central (0–5%) collisions. It is observed that the AMPT results reasonably describe the experimental data. The AMPT results of $\epsilon_{\rm Bj}\tau$ are fitted with a power law (for central $\propto s^{0.22\pm0.015}$) for different centralities. For central (0–5%) collisions, the value of $\epsilon_{\rm Bj}\tau$ comes out to

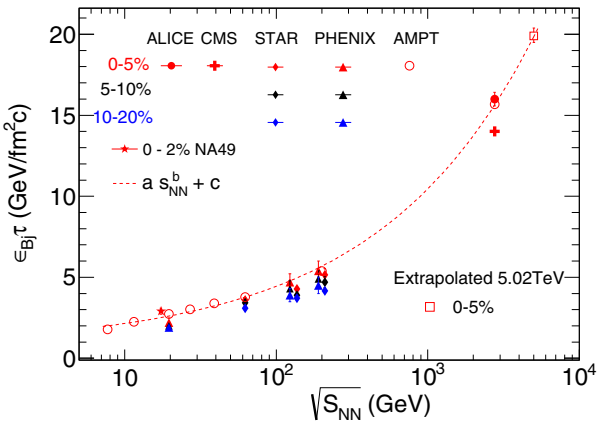

FIG. 7. Energy density ($\epsilon_{\mathrm{Bj}}\tau$) as a function of $\sqrt{s_{NN}}$ for experimental data [15,31–38] and the AMPT model data. Power-law fits to the AMPT results are extrapolated to $\sqrt{s_{NN}} = 5.02$ TeV. Some of the data points are shifted along the x axis for clarity of presentation.

be 19.88 ± 0.48 GeV/fm^2 c. The value of the exponent in the power-law fits are observed to vary from $s_{NN}^{0.22}$ to $s_{NN}^{0.10}$ for central (0–5%) to peripheral (70–80%) collisions, respectively. $\epsilon_{\mathrm{Bj}}\tau$ is a combination of $dN_{\mathrm{ch}}/d\eta$ and $\langle m_{\mathrm{T}}\rangle$, both of which vary as power law with respect to collision energy. That may explain the origin of the power-law behavior of the energy density. As a function of collision energy, the energy density increases much faster for central collisions compared to peripheral collisions.

VI. SUMMARY

We have studied the η distributions of produced charged particles for Au + Au collisions at $\sqrt{s_{NN}} = 7.7$ to 200 GeV, corresponding to the collisions at the RHIC and for Pb + Pb collisions at $\sqrt{s_{NN}} = 2.76$ TeV, corresponding to the collisions at the LHC. We have employed the SM mode of the AMPT model to describe the experimental data. We observe that using the total parton elastic cross section, $\sigma_{\mathrm{gg}} = 10$ mb, the AMPT model can explain the RHIC data, whereas $\sigma_{\mathrm{gg}} = 1.5$ mb is needed for explaining the data at the LHC. The AMPT model with these settings is used to further study the η distributions and initial energy densities. The shapes of the η distributions could be explained by using double Gaussian functions with a set of parameters comprising the amplitude, the position of the peaks in η, and the widths of the distributions. As expected, with the increase of the beam energy, the amplitudes increase, the peak positions move farther apart, and the widths of the distributions increase. The parameters are fitted well by power-law fits, through which the pseudorapidity distributions can be obtained for any beam energy and collision centrality. We obtain the initial energy density as a function of collision energy and collision centrality using Bjorken formalism. Power-law fits to the multiplicity density at midrapidity give the s_{NN} dependence as $s_{NN}^{0.154}$ to $s_{NN}^{0.109}$ from top central (0–5%) to peripheral (70–80%) collisions. Similarly, power-law fits to the energy density yield the s_{NN} dependence as $s_{NN}^{0.22}$ to $s_{NN}^{0.10}$ for the same centrality ranges. As a function of collision energy, the particle multiplicity and energy density increase much faster for central collisions compared to the peripheral collisions. Extrapolating the parameters to collisions at $\sqrt{s_{NN}} = 5.02$ TeV, we are able to explain the recently published results on the centrality dependence of charged-particle multiplicity and energy density. At this energy, the pseudorapidity density of charged particles for central (0–5%) collisions is 1964 ± 30 and the energy density $\epsilon_{\mathrm{Bj}}\tau$ is 19.98 GeV/fm^2 c. Furthermore, we note that the results obtained in the present study can be interpolated for intermediate energies to obtain η distributions and energy densities for heavy-ion collisions at the Facility for Antiproton and Ion Research (FAIR). For a laboratory energy of 11 GeV at the FAIR, the energy density would be 1.8 GeV/fm^3 for $\tau = 1$ fm, which is an interesting region in which to study the deconfined matter at high net-baryon density.

ACKNOWLEDGMENT

This research used resources of the LHC Grid Computing Center at the Variable Energy Cyclotron Centre.

[1] J. W. Harris and B. Muller, Annu. Rev. Nucl. Part. Sci. **46**, 71 (1996).
[2] P. Braun-Munzinger and J. Stachel, Nature (London) **448**, 302 (2007).
[3] A. Bazavov, T. Bhattacharya, C. DeTar, H. T. Ding, S. Gottlieb, R. Gupta, P. Hegde, U. M. Heller, F. Karsch, E. Laermann, L. Levkova, S. Mukherjee, P. Petreczky, C. Schmidt, C. Schroeder, R. A. Soltz, W. Soeldner, R. Sugar, M. Wagner, and P. Vranas, Phys. Rev. D **90**, 094503 (2014).
[4] Y. Aoki *et al.*, J. High Energy Phys. 06 (2009) 088.
[5] M. M. Aggarwal *et al.* (STAR Collaboration), arXiv:1007.2613.
[6] S. Ozonder and R. J. Fries, Phys. Rev. C **89**, 034902 (2014).
[7] J. Dias de Deus and R. Ugoccioni, Phys. Lett. B **494**, 53 (2000).
[8] J. Zhi-jin and S. Yu-Fen, Chin. Phys. Lett. **29**, 022502 (2012).
[9] L. Zhou and G. S. F. Stephans, Phys. Rev. C **90**, 014902 (2014).
[10] F. I. Shao, T. Yao, and Q. Xie, Phys. Rev. **75**, 034904 (2007).
[11] M. Kliemant, R. Sahoo, T. Schuster, and R. Stock, *The Physics of the Quark-Gluon Plasma*, edited by S. Sarkar, H. Satz, and B. Sinha, Lecture Notes in Physics Vol. 785 (Springer, New York, 2009), pp. 23–103.
[12] R. Sahoo, A. N. Mishra, N. K. Behera, and B. K. Nandi, Adv. High Energy Phys. **2015**, 612390 (2015).
[13] J. D. Bjorken, Phys. Rev. D **27**, 140 (1983).
[14] B. Alver *et al.* (PHOBOS Collaboration), Phys. Rev. C **83**, 024913 (2011).
[15] B. Abelev *et al.* (STAR Collaboration), Phys. Rev. C **79**, 034909 (2009).
[16] E. Abbas *et al.* (ALICE Collaboration), Phys. Lett. B **726**, 610 (2013).
[17] J. Adam *et al.* (ALICE Collaboration), Phys. Lett. B **754**, 373 (2016).
[18] Y. Chen *et al.* (ATLAS Collaboration), J. Phys. G **38**, 124042 (2011).

[19] G. Aad *et al.* (ATLAS Collaboration), Phys. Lett. B **710**, 363 (2012).
[20] S. Chatrchyan *et al.* (CMS Collaboration), J. High Energy Phys. 08 (2011) 141.
[21] J. Adam *et al.* (ALICE Collaboration), arXiv:1512.06104.
[22] Z. W. Lin, C. M. Ko, B. A. Li, B. Zhang, and S. Pal, Phys. Rev. C **72**, 064901 (2005).
[23] Z. W. Lin, arXiv:1403.1854.
[24] S. Pal and M. Bleicher, Phys. Lett. B **709**, 82 (2012).
[25] J. Xu and C. M. Ko, Phys. Rev. C **84**, 014903 (2011).
[26] X.-N. Wang and M. Gyulassy, Phys. Rev. D **44**, 3501 (1991).
[27] B. Li, A. T. Sustich, B. Zhang, and C. M. Ko, Int. J. Mod. Phys. E **10**, 267 (2001).
[28] R. J. Fries, V. Greco, and P. Sorensen, Annu. Rev. Nucl. Part. Sci. **58**, 177 (2008).
[29] R. J. Fries, B. Muller, C. Nonaka, and S. A. Bass, Phys. Rev. Lett. **90**, 202303 (2003).
[30] D. Solanki, P. Sorensen, S. Basu, R. Raniwala, and T. K. Nayak, Phys. Lett. B **720**, 352 (2013).
[31] K. Adcox *et al.* (PHENIX Collaboration), Phys. Rev. Lett. **87**, 052301 (2001).
[32] T. Alber *et al.*, Phys. Rev. Lett. **75**, 3814 (1995).
[33] J. Adam *et al.* (STAR Collaboration), Phys. Rev. C **70**, 054907 (2004).
[34] S. S. Adler *et al.* (PHENIX Collaboration), Phys. Rev. C **71**, 034908 (2005).
[35] J. T. Mitchell *et al.* (PHENIX Collaboration), Nucl. Phys. A (to be published) [arXiv:1601.00904].
[36] C. Loizides *et al.* (ALICE Collaboration), J. Phys. G **38**, 124040 (2011).
[37] A. Toia *et al.* (ALICE Collaboration), J. Phys. G **38**, 124007 (2011).
[38] S. Chatrchyan *et al.* (CMS Collaboration), Phys. Rev. Lett. **109**, 152303 (2012).